CRYSTAL GROWTH & DESIGN

pubs.acs.org/crystal

Article

Impact of Growth Environment on the Crystal Growth and Magnetic and Electronic Properties of Ba_2NiWO_6 Single Crystals

Abanoub R. N. Hanna,* A. T. M. Nazmul Islam, Daniel Abou-Ras, Clemes Ritter, Igal Levine, Ralf Feyerherm, and Bella Lake*

Cite This: *Cryst. Growth Des.* 2025, 25, 1155−1163

Read Online

ACCESS | Metrics & More | Article Recommendations | Supporting Information

ABSTRACT: This study introduces the effect of growth atmosphere and pressure on the as-grown crystals and the physical characterization of the double perovskite compound Ba_2NiWO_6 (BNWO). The Ni^{2+} ions form a face-centered cubic (FCC) lattice with an ideal octahedral arrangement. Our growth trials by the floating zone method revealed that BNWO exhibits two distinct colors depending on the growth atmosphere, suggesting that it influences its stoichiometry and phase purity. The antiferromagnetic properties of BNWO align with conventional antiferromagnetic behavior with a $J = 1$ ground state, as determined by entropy calculation. Additionally, surface photovoltage (SPV) spectroscopy indicates that the impurity levels within the crystal influence the electronic properties of BNWO.

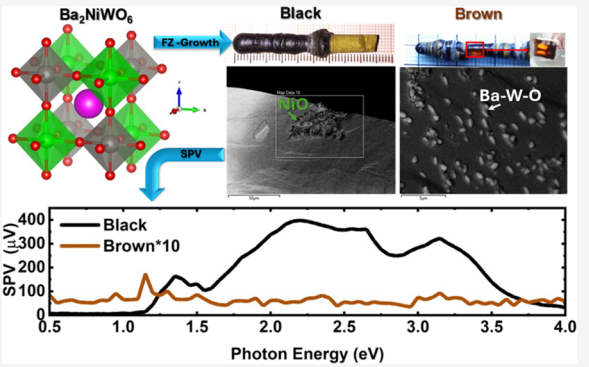

INTRODUCTION

Cubic double perovskite compounds exhibit unique structural properties and a high degree of atomic ordering. This has piqued the interest of scientists, leading to extensive research in various fields, especially for fundamental studies on quantum magnetism and colossal magnetoresistance.[1−4] Additionally, their crystal structures with high symmetry and almost ideal octahedral arrangements around the metal cations are typically suited for modifying electronic properties, thereby enabling applications in photocatalysis, optoelectronics, and solar cells.[5−8]

The crystal chemistry features of the double perovskites play a crucial role in determining their properties and functionalities. Double perovskites are characterized by the formula $A_2BB'O_6$ and consist of a three-dimensional network of corner-sharing BO_6 octahedra, where B represents a metal cation. The B' cation resides at the center of the octahedra, and its size and charge balance have a direct impact on the overall stability and electronic properties of the material. The arrangement of magnetic ions in the B site forms a face-centered cubic (FCC) sublattice of the magnetic ions. A widespread range of magnetic properties were reported in such compounds including ferromagnetic, antiferromagnetic, and frustrated magnetism.[4,5,9,10] However, realizing these fascinating properties requires a high-quality single crystal for physical property measurements.

The floating zone method is essential for growing high-quality single crystals of double perovskite compounds, which are vital for accurate physical property measurements.[11−13] This technique avoids contamination by eliminating the need for a crucible or heating element, resulting in high-quality crystals. It is versatile, accommodating various materials, and allows for the growth of large, structurally sound crystals with precise control over growth parameters. The significance of the floating zone method lies in its ability to produce high-quality crystals that enhance the accuracy and reliability of research in materials science and condensed matter physics.[13−15]

Herein, we provide a comprehensive explanation of the crystal growth and characterization of the physical and electronic properties of the double perovskite compound Ba_2NiWO_6 (BNWO), where the Ni^{2+} ions form an FCC lattice with an ideal octahedral arrangement as shown in Figure 1. The growth trials revealed that the BNWO has two different colors depending on the growth atmosphere, which in turn affects the stoichiometry and phase purity. The antiferromagnetic properties of BNWO can be described as conventional antiferromagnetic behavior. The surface photovoltage (SPV) spectroscopy indicates that the electronic properties of BNWO are also affected by the growth atmosphere and depend on the percentage of impurities in the crystal.

Received: October 24, 2024
Revised: January 29, 2025
Accepted: January 30, 2025
Published: February 7, 2025

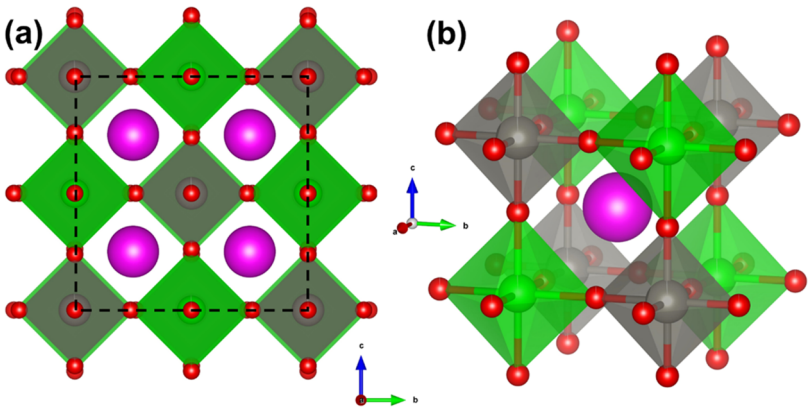

Figure 1. Unit cell of the double perovskite Ba_2NiWO_6 (BNWO) consists of Ni^{2+} ions (green) surrounded by six O^{2-} ions (red) forming an octahedron, as well as Ba^{2+} (purple) and W^{6+} (gray) ions. (a) The projection onto the *ab*-plane. (b) The arrangement of Ni^{2+} and W^{6+} ions in the ideal octahedral geometry.

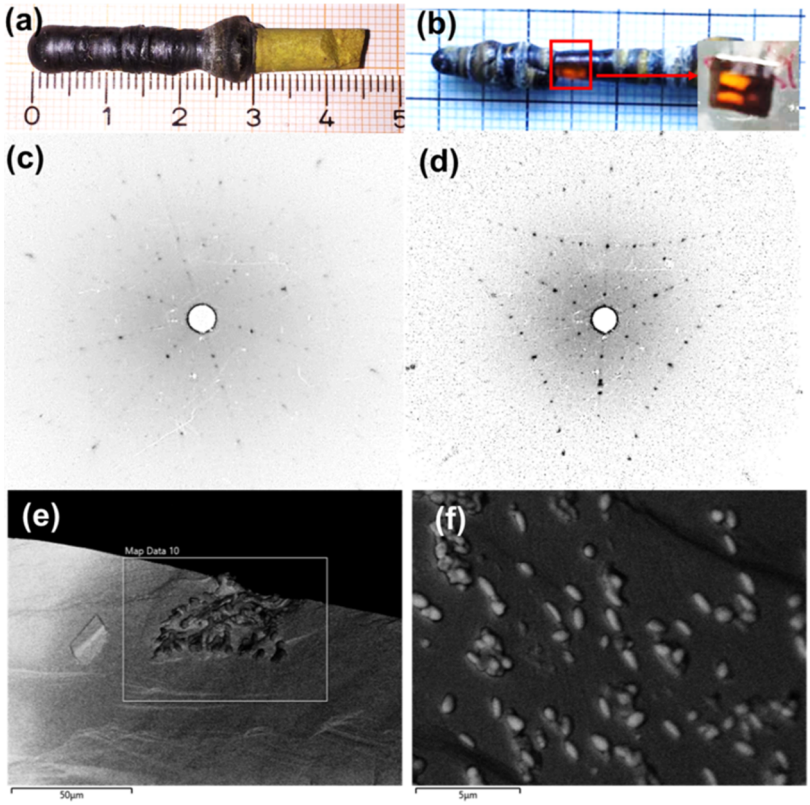

Figure 2. Grown crystals of Ba_2NiWO_6: (a) premelted feed rod in ambient conditions yielding opaque black crystals. (b) Growth trial under a 2 bar argon atmosphere yielding transparent brown crystals. (c, d) Laue diffraction patterns for the black and brown crystals along the ⟨110⟩ and ⟨111⟩ symmetries, respectively. (e, f) SEM images of the black and brown crystals, respectively, indicating the impurity phases, grains, and defects on the surface of each crystal.

EXPERIMENTAL DETAILS

BNWO was prepared in powder form using the solid-state reaction method as previously described.[16,17] The precursors ($BaCO_3$, NiO, WO_3) (99.99%, Alfa Aesar) were mixed in a stoichiometric ratio and heated in several steps to 900, 1200, and 1350 °C in air for 12 h each with intermediate grindings. BNWO was obtained as a yellowish-green powder.

Single crystals of BNWO were grown by using the optical floating zone (FZ) technique. The crystal growth was performed using a 4-mirror infrared image furnace (Crystal Systems Corp., FZ-T-10000-H-VI-VP) at the CoreLab Quantum Materials (CLQM) at the Helmholtz Zentrum Berlin für Materialien and Energie (HZB), Germany. High-density feed rods were prepared by packing BNWO powder in a rubber tube and subjecting it to a pressure of 2000 bar in a cold isostatic press (CIP) machine, yielding a uniform cylindrical rod with dimensions of roughly 70 mm length and 5 mm diameter. The rod was sintered in air for 12 h at 1350 °C and used as a feed for crystal growth. 300 W lamps were used for the growth, and a small part of the rod was used as a seed to initiate the growth. The rotation rate was 5−6 rpm for the upper shaft and 10−15 rpm for the lower shaft.

The structural characterization and phase purity were conducted using both powder X-ray diffraction (PXRD) by a Bruker D8 XRD diffractometer equipped with a copper source Kα X-ray (wavelength λ = 1.542 Å) at the CLQM at HZB. Neutron powder diffraction (NPD) was also performed at the D2B neutron diffraction with incident

https://doi.org/10.1021/acs.cgd.4c01467
Cryst. Growth Des. 2025, 25, 1155−1163

neutron wavelength λ = 1.594 Å at the Institut Laue-Langevin (ILL), France. Measurements were performed on both crushed single crystals and the powder obtained by a solid-state reaction at room temperature. For the NPD measurement, the weight of the samples was about 3.5 g.

The crystals were systematically investigated and mapped using a Laue Diffraction Camera and aligned to the crystallographic directions for physical property measurements. The Laue spots were solid and clear, representing the quality of the crystals as shown in Figure 2b,c.

Elemental analysis by energy-dispersive X-ray (EDX) spectrometry was carried out using a Zeiss Merlin scanning electron microscope (SEM) at the HZB.

X-ray photoelectron spectroscopy (XPS) analyses were performed using a monochromatic Al Kα X-ray source (Focus 500, Specs), with a photon energy of 1486.84 eV and an electron analyzer (Phoibos 100, Specs) at the Institute of Solar Fuels, HZB.

The physical properties of the single crystal of BNWO were analyzed using both the Physical Property Measurement System (PPMS) and SQUID magnetometer (MPMS) at HZB. The magnetization and heat capacity were measured up to 90 kOe over a temperature range of 2−400 K at the CLQM.

The optical properties of the different phases were probed using surface photovoltage (SPV) spectroscopy at room temperature.[18] SPV was measured by the fixed capacitor method using a chopper with a frequency of 8 Hz for both single crystal and powder in the photon energy range of 0.5−5 eV.

Crystal Growth. Our initial melting trials of the stoichiometric powder by FZ growth indicated that BNWO melts incongruently. The decomposition of BNWO above 1200 °C was indicated by the presence of $BaWO_4$ as a secondary phase.[19] The presence of $BaWO_4$ is attributed to a change in the stoichiometry. Our investigation indicated that the complete melting of BNWO occurs at 1560 °C. The slow cooling of the melt yielded a mixture of phases Ba_2NiWO_6 in the form of dark brown crystals and brown melt containing a mixture of phases: Ba_2NiWO_6, Ba_2WO_5, $BaWO_4$, and NiO with different fractions depending on the cooling rate and melting conditions. Despite the possibility of growth by the self-flux method from the BNWO melt at 1560 °C, the crystals were relatively small (≈2 mm^3) and had some impurities in their matrix. Therefore, it was particularly challenging to optimize the growth conditions and obtain a relatively large crystal.

As a result of the incongruent melting nature of BNWO, most of the growth trials by FZ were unstable, and we could not stabilize the growth beyond a length of more than 6 mm. Structural analysis showed that most of the crystals grown had impurities, including those grown by slow cooling. The impurities are mainly Ba_2WO_5, $BaWO_4$, and NiO with different percentages depending on the growth conditions.

To improve the quality of the crystal, we tried several things. First, we performed a fast zone pass of the feed rod to improve the density. In this step, the feed rod was melted at a very high rate (>30 mm/h). The quick melting provided denser feed rods with fewer air bubbles for growth trials. Nevertheless, the growth was quite unstable and zone breaking occurred many times owing to the accumulation of NiO in the molten zone. NiO segregates and solidifies in the zone causing unstable growth. We were able to stabilize the growth over 20 mm with a growth rate of 4 mm/h and a power of 90% of 300 W lamps. The grown crystals are shown in Figure 2a. The grown crystal was ca. 15 mm with a purity of 97.1% (by XRD diffraction), and the major impurity was the nonmagnetic phase Ba_2WO_5 (2.8%). NiO was undetectable by PXRD in the crystal, but it was found in excess at the melt zone.

To avoid the segregation of NiO, we also performed growth experiments under different growth atmospheres in the furnace. The powder preparation and crystal growth trials were performed in air at ambient pressure. However, the incongruent melting nature that destabilizes the growth and allows the impurity phase to form might change in the absence of oxygen or by applying pressure. Therefore, we conducted growth trials under an argon atmosphere and applied pressure up to 2 bar to see if the melting nature would improve. Although most growth trials were unstable, the growth under 2 bar of argon pressure yielded a transparent brown crystal of BNWO using a growth rate of 1 mm/h and a power of 90% of 300 W lamps, as shown in Figure 2b.

Using a reductive atmosphere is critical since it may also affect tungsten (W^{6+}), which can occupy many different oxidation states, and the most common ones are 4+ and 6+. While the W^{6+} is nonmagnetic and has no contribution to the magnetic properties of the sample, W^{4+} is magnetic and might interact with the Ni^{2+} spins and contribute to the magnetic properties. Nevertheless, we found that W remains W^{6+} in all cases. This result is supported by structural characterization (XRD, XPS) and magnetic measurements, which showed no behavior related to W^{4+}. In this context, we also mention that the site mixing of W^{6+} and Ni^{2+} is less likely to occur due to the different oxidation states, ionic radii, and the relatively slow growth rate (≤2 mm/h) during the growth experiments.

The reason behind the color difference between the two crystals could be attributed to a change in the nickel valence or the impurities when the growth occurs in air or argon. To test that, we annealed small pieces of the black crystals, which were grown in air, under an argon atmosphere near the melting temperature of 1560 °C. We found that some parts of the annealed pieces changed to transparent brown. This finding suggests that the different colors are caused by a change in the oxygen stoichiometry.

To achieve more stable growth, we tried the traveling solvent floating zone (TSFZ) method using different solvents containing excess WO_3 and BaO according to the phase diagram (see Figure S1). We also performed the growth under both argon and oxygen atmospheres as well as different pressures. None of these trials were successful. The melting of the solvents is much lower under the argon atmosphere, and the solvents were unable to dissolve BNWO at a lower temperature than its melting temperature.

RESULTS

Structural Characterization. The structural parameters and phase purity of the polycrystalline and single-crystalline phases of BNWO were first inspected by room-temperature powder X-ray diffraction (PXRD). The PXRD data were refined by *FullProf* software using the Rietveld refinement to extract the structural parameters and the volume fraction of each phase.[20] The main phases were refined using the $Fm\bar{3}m$ space group (No. 225). The refinement factors are summarized for both powder and the crushed black and brown crystals of BNWO in the Supporting Information (see Figure S2 and Table S1).

Cubic BNWO is rock-salt-ordered, consisting of regular BaO_{12} cuboctahedra and corner-sharing regular NiO_6 and WO_6 octahedra. Due to the similar size, ions located on the B sites of the double perovskite structure are allowed to occupy the antisites of each other. Ba^{2+} occupies the *8c* position, while Ni^{2+} occupies the *4b* positions, W^{6+} occupies the *4a* position, and O^{2-} occupies the *24e* position. These atomic positions are fixed by symmetry, except for oxygen. The refinement of the powder XRD pattern showed the presence of an impurity phase Ba_2WO_5 (space group $P21/n$). However, the calculated stoichiometry is not reliable since X-ray diffraction is insensitive to oxygen compared to heavier ions such as W, Ni, and Ba. Furthermore, only 24 positions per unit cell are allowed for oxygen atoms (or 6 oxygen atoms per formula unit). Nevertheless, the apparent color difference of the samples can be interpreted as indicative of the presence of impurities or point defects that cannot be detected by conventional XRD.

On the other hand, the phenomenon of different crystal colors is reported for many compounds containing nickel, due to the possible oxidation states of nickel, which can change

https://doi.org/10.1021/acs.cgd.4c01467
Cryst. Growth Des. 2025, 25, 1155−1163

from Ni^{2+} to Ni^{3+}, as Ni^{3+} is stable at high temperatures.[21−23] However, we did not find any solid evidence indicating the presence of Ni^{3+} in our samples. We performed X-ray photoelectron spectroscopy (XPS) analyses to detect any absorption from both Ni^{2+} and Ni^{3+} in the crystals, but no absorption peaks related to Ni^{3+} or W^{4+} were detected as shown in Figure S3. Nevertheless, the peaks are slightly shifted by a constant offset (25 eV), which indicates a difference between the two samples.

To test the possibility of different stoichiometries, defects, and oxygen contents in the samples, we used energy-dispersive X-ray (EDX) spectrometry to estimate the atomic percentage of oxygen in the black and brown crystals. We found that the brown sample exhibits Ba-/W-rich, Ni-poor phases on the surface, but their atomic percents are within the error of measurement (1−2 atom %). The elemental concentrations in the matrix agreed well with the expected precipitates (Ba_2WO_5, NiO, and $BaWO_4$), which appear as grains and surface defects, as shown in Figure 2f. In contrast, for the black sample, the detected precipitates are from stoichiometric (Ba_2NiWO_6) and Ni-rich (Ni−O) phases as islands on the surface, as shown in Figure 2e. The results of atomic percents are summarized in Table S2.

To get more precise results of the impurity phases and oxygen contents, the structural parameters, and phase purity of the poly- and single-crystalline phases of BNWO, they were further investigated using neutron powder diffraction (NPD) at room temperature. The brown crystal was relatively small, so we could not perform NPD on it but rather on a powder sample sintered under argon for 5 days until it turned brown. The refinement of the neutron diffraction patterns indicated the presence of different impurities in different samples. The black crystal was found to have an impurity phase of 1.29% NiO (weight fraction). The brown sample has a mixture of impurities: 0.26% NiO, 5.37% Ba_2WO_5, and 2.34% $BaWO_4$. These results support the EDX data showing the Ba-/W-rich phases on the surface of the brown crystal. The as-prepared powder has 1.76% NiO and 5.98% $BaWO_4$. These numbers represent the weight fraction of each phase and provide strong evidence for the difference between the three samples as shown in Figure 3 and summarized in Table 1. The occupancy of oxygen was accurately determined in each sample and did not show any oxygen deficiency in the samples. Altogether, the results indicate the superior quality of the black crystal with fewer impurities compared to that of the brown crystal.

To investigate the possibility of site disorder, we carefully checked the reflections that are most sensitive to cation site order/disorder ⟨111⟩, ⟨311⟩, and ⟨331⟩ reflections, which appear at approximately 13, 25, and 33°. These reflections are well-fit under the assumption of no site disorder between the *4a* and *4b* sites. Attempting to refine the model with a fixed 10% cation disorder leads to significant deviations in these reflections. We also conducted a refinement focused on site order/disorder. The results indicated no significant site disorder between Ni and W at the sites *4a* ⟨000⟩ and *4b* ⟨1/2 1/2 1/2⟩, yielding a disorder value of only 0.2(8)%.

Magnetization. As mentioned in the Structural Characterization section, the black and brown crystals of BNWO are different in terms of stoichiometry and impurities. Consequently, the magnetic properties of the two crystals might not be the same. Figure 4a shows the difference in the temperature dependence of the magnetic susceptibility of the crystals for an applied field of 10 kOe along the ⟨110⟩ direction. The black crystal has a lower magnetic susceptibility, indicating that the excess Ni^{2+} ions from the NiO impurity suppress the total moment of the black crystal. The inverse susceptibility of the black crystal deviates from linear behavior above 250 K, indicating a possible contribution from NiO impurity, which orders antiferromagnetically at T = 523 K and exhibits a curvature of $1/\chi$ at T > 150 K.[24] We tried to apply a universal scaling factor to both samples to check whether they have identical magnetic behavior, but it was not feasible due to the nonlinear inverse susceptibility of the black crystal. Nevertheless, the Néel temperature T_N is still the same in the two crystals. Therefore, we proceeded with measurements of the brown crystal since it has a smaller percentage of magnetic impurities.

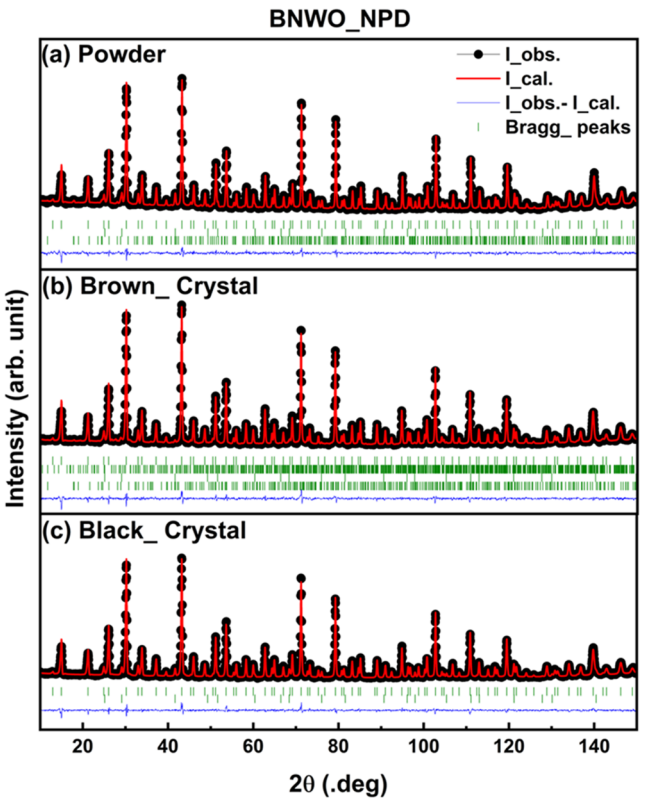

Figure 3. Rietveld refinement of the neutron powder diffraction of BNWO: (a) as-prepared BNWO powder, (b) brown crystal, and (c) black crystal. The data are represented by the black circles, the fit is represented by the red line, and the difference between them is represented by the blue line. The vertical green lines represent the phases in each sample: the powder has three phases: 92.35% BNWO, 1.67% NiO, and 5.98% $BaWO_4$. The brown crystal has four phases: 92.02% BNWO, 5.37% Ba_2WO_5, 0.26% NiO, and 2.34% $BaWO_4$. The black crystal has two phases: 98.7% BNWO and 1.29% NiO. The refinement parameters and percentage of impurities are summarized in Table 1.

Figure 4b shows the temperature dependence of the inverse susceptibility of the BNWO brown crystal for fields along the ⟨110⟩ and ⟨111⟩ crystallographic directions. The magnetic susceptibility for the magnetic field applied along different directions of the BNWO crystal indicated antiferromagnetic order at T_N= 47(1) K. T_N was determined from the maximum of the first derivative of the susceptibility data as shown in Figure 4c. The Néel temperature agrees with the previously reported data for powder samples (48 K).[7,25] The temperature dependence of the magnetic susceptibility for different

https://doi.org/10.1021/acs.cgd.4c01467
Cryst. Growth Des. 2025, 25, 1155−1163

Table 1. Rietveld Refinement Parameters for NPD of BNWO Samples, Including the Weight Fraction of BNWO, NiO, and B−W−O Phases in Each Sample, the Lattice Parameter (a), the Expected *R*-Factor (R_{exp}), the Goodness of Fit (χ^2), the Atomic Positions of Oxygen in the *x* Direction (O_x), and the Occupancy of Oxygen Atoms (O_{occ})

BNWO	BNWO (%)	NiO (%)	Ba−W−O (%)	*a* (Å)	R_{exp} (%)	χ^2	O_x	O_{occ} (%)
black	98.70(86)	1.29(03)	0.01	8.06692(61)	3.52	1.56	0.2387(1)	99.76
brown	92.02(96)	0.26(03)	7.72(41)	8.06689(50)	3.45	1.70	0.2389(1)	100.56
powder	92.35(97)	1.76(04)	5.98(35)	8.06626	3.15	1.44	0.239(1)	99.92
reported[3]	100.00	0	0	8.0679	10.1	1.50	0.25	100.00

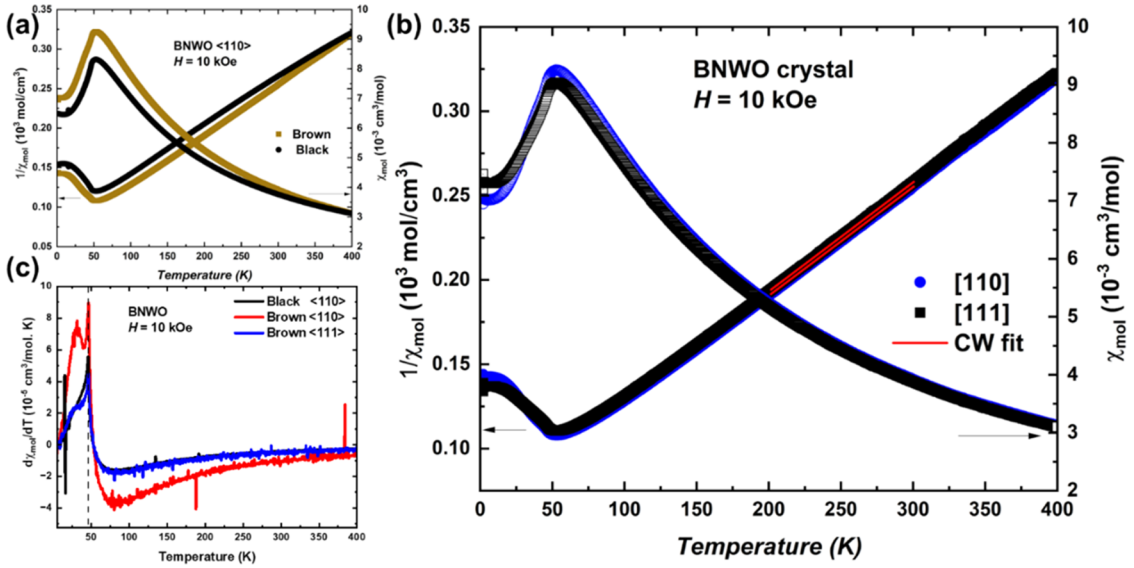

Figure 4. Temperature dependence of magnetic susceptibility (left) and inverse susceptibility (right). (a) BNWO black and brown crystals for the ⟨110⟩ direction at 10 kOe. (b) BNWO brown crystal for ⟨110⟩ (blue circles) and ⟨111⟩ (black squares) directions at 10 kOe; the red line gives the Curie−Weiss fit. The field dependence of the inverse susceptibility reveals a weak anisotropy below T_N. (c) The first derivative of magnetic susceptibility of the black and brown crystals at 10 kOe indicating the Neel temperature T_N = 47 K.

Table 2. Fitting Values for the Inverse Susceptibility of BNWO Crystals According to the Curie−Weiss Model[a]

	H =1 kOe			*H* = 10 kOe		
Ba_2NiWO_6, 200−300 K	Θ_{CW}	μ_{eff}	*g*	Θ_{CW}	μ_{eff}	*g*
⟨110⟩ black	−118.0(1)	3.6(1)	2.5	−117.0(1)	3.7(1)	2.6
⟨110⟩ brown	−99.6(1)	3.5(1)	2.5	−96.2(1)	3.5(1)	2.5
⟨111⟩ brown	−108.0(1)	3.6(1)	2.5	−99.2(1)	3.5(1)	2.5

[a]*H* Is the applied magnetic field in Oersted, Θ_{CW} is the Curie−Weiss temperature in K, μ_{eff} is the effective moment in μ_B, and *g* Is the Lande *g* factor.

crystallographic directions showed similar behavior, suggesting that the magnetism is almost isotropic. Therefore, BNWO can be considered an isotropic magnet. A very weak anisotropy exists below T_N. The weak anisotropy may indicate that in the AF ordered state the ordered moments point closer to ⟨110⟩ than to ⟨111⟩ direction, since the susceptibility is slightly lower for the ⟨110⟩ direction.

The inverse susceptibility data were fitted by using the Curie−Weiss (CW) model. The fitting parameters including the Curie−Weiss temperature (Θ_{CW}), effective moment (μ_{eff}), and g factor are summarized in Table 2 for different directions and different applied fields. The black crystal has slightly higher fitting values, probably due to the contribution of NiO to the total magnetization. The CW fitting of the single-crystal data gives a range of values for Θ_{CW} between −94.4 and −118 K and the effective moment μ_{eff} = 3.48−3.60 μ_B for the fitted temperature range of 200−300 K. Θ_{CW} and μ_{eff} were insensitive to the temperature range above 100 K, and fitting in the temperature range of 100−400 or 200−300 K gives the same fitted values for Θ_{CW} and μ_{eff}. The value of the effective moment is larger than the spin-only moment of $S = 1$ (2.83 μ_B) but lies within the experimental range of similar Ni^{2+} compounds.[26]

The *g* value was calculated according to the equation $\mu_{eff} = g_J \mu_B \sqrt{J(J+1)}$ assuming spin-only contribution ($J = S$) for Ni^{2+} with $S = 1$. The *g* value (2.43−2.53) is higher than the expected value ($g = 2$). This high value suggests that the magnetic moment might not be solely attributable to the spin-only contribution but rather suggests a small orbital contribution.

Isothermal magnetization measurements provide evidence for a possible weak anisotropy and the spin direction in BNWO. Figure 5 represents the magnetization curves, while the first derivative of magnetization for different crystallographic directions is shown in the inset. The measurement elucidates that the magnetization of BNWO has nonlinear

https://doi.org/10.1021/acs.cgd.4c01467
Cryst. Growth Des. 2025, 25, 1155−1163

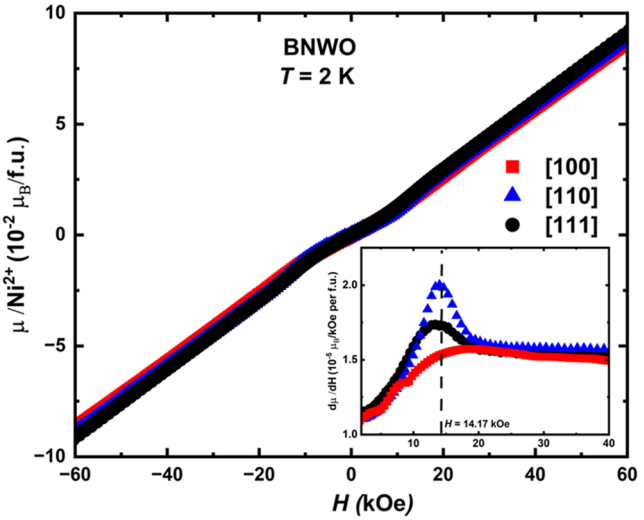

Figure 5. Isothermal magnetization for different directions of the BNWO crystals. The inset shows the derivative of the field-induced moment per Ni^{2+} ion for the directions ⟨100⟩ (red), ⟨110⟩ (blue), and ⟨111⟩ (black). The dashed line indicates a spin-flop transition around 14 kOe for ⟨110⟩ and ⟨111⟩ directions, while the signal of the ⟨100⟩ direction is much broader, indicating that the spin-flop transition is weaker or absent, suggesting that the spins might have a preferred orientation.

behavior for all three directions. The first derivative of magnetization of ⟨110⟩ and ⟨111⟩ indicated a peak at 14 kOe representing a spin-flop transition. The ⟨110⟩ direction shows the sharpest peak. The spin-flop transition indicates a weak anisotropy in the system in certain directions where the AFM ordered magnetic spins rotate to a direction perpendicular to the field direction to minimize the total energy.[27] For the ⟨100⟩ direction, the derivative of magnetization is much broader, indicating a weaker or absent spin-flop transition along ⟨100⟩. Altogether, these results suggest that the spins in BNWO point perpendicular to the ⟨100⟩ direction and lie close to the ⟨110⟩ direction with a component along ⟨111⟩.

Heat Capacity. The temperature dependence of the heat capacity of the brown crystal of BNWO is shown in Figure 6 in zero field and for the applied magnetic field along the ⟨110⟩ direction. The measurement indicated the second-order phase transition at 46 K attributed to the long-range antiferromagnetic order in agreement with the magnetic susceptibility data. No significant change was observed in the heat capacity under different applied magnetic fields up to 90 kOe, and the Néel temperature is almost field-independent, as shown in the inset of Figure 6a. The magnetic contribution of the heat capacity was extracted by modeling the phonon contribution using a combination of Debye and Einstein models (D−E). The temperature range of 70−180 K was used for the fitting with the sum of one Debye mode and one Einstein mode according to the equation

$$C_p(T) = 3Rn\left(p_D\left(\frac{T}{\theta_D}\right)^3 3\int_0^{\theta_D/T}\frac{x^4 e^x}{(e^x-1)^2}dx + (1-p_D)\left(\frac{\theta_E}{T}\right)^2\frac{e^{\theta_E/T}}{(e^{\theta_E/T}-1)^2}\right)$$

where R is the universal gas constant, n is the number of ions per formula unit, which is 10 for BNWO, p_D is the weighting of the Debye mode, and θ_D and θ_E are the Debye and Einstein temperatures, respectively.

The model suggests the Debye temperature θ_D = 299 (1) K and Einstein temperature θ_E = 690 (3) K with p_D = 0.44(1). The extracted magnetic heat capacity, c_{mag}, and entropy changes are shown in Figure 6b.

The magnetic entropy was determined by integrating c_{mag}/T over temperatures up to 100 K. The entropy in the range of 2−100 K is 8.9 J/mol·K, which is 0.97 Rln3, where Rln3 is the expected value for $J = S = 1$. Therefore, the entropy calculations suggest a J = 1 ground state of the Ni^{2+} ions in BNWO. This result supports the susceptibility measurements, suggesting a spin-only magnetic moment and a weak orbital contribution.

Electronic Structure. Many previous reports calculated the band structure of BNWO using different theoretical

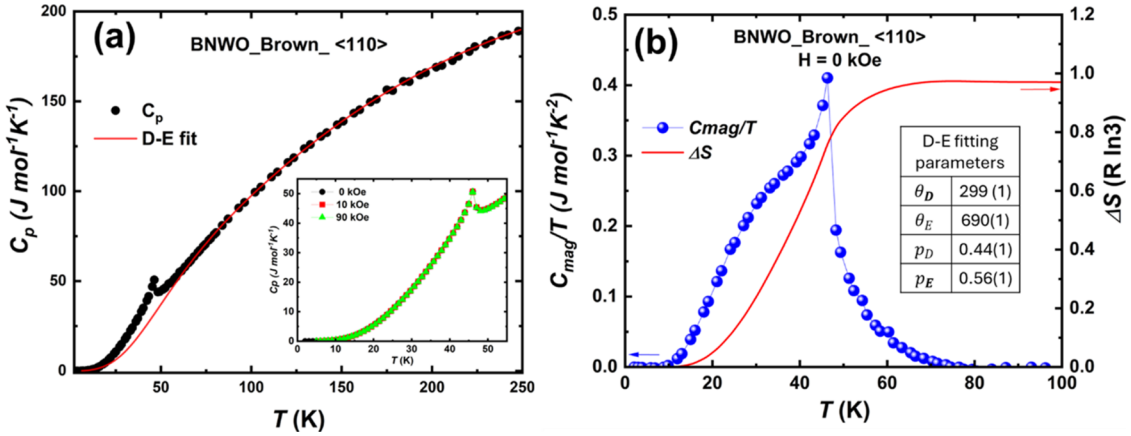

Figure 6. (a) Temperature dependence of the heat capacity of the BNWO brown crystal in the zero field (black dot). The magnetic contribution was extracted by modeling the nonmagnetic contributions using the Debye and Einstein models (red line). The inset represents the low-temperature heat capacity in the zero field and for the field up to 90 kOe applied along the ⟨110⟩ direction. (b) Magnetic contribution of the heat capacity over the temperature of the brown crystal at the zero field. The magnetic contribution was obtained by subtracting the modeled lattice contribution, and the fitting parameters are listed in the inset. The change in entropy is shown on the left axis in units of Rln3.

https://doi.org/10.1021/acs.cgd.4c01467
Cryst. Growth Des. 2025, 25, 1155−1163

models.[3,7,19,28] Some reports suggested that BNWO has an indirect band gap at 2.48 eV and would be transparent in the visible domain.[7] An indirect band gap makes electron excitation less efficient compared to direct band-gap materials. Experimental investigations using diffuse reflectance spectroscopy indicated a wide band gap at 3.29 eV.[29] To compare our samples with previous reports, we measured the surface photovoltage of both the polycrystalline and single crystals, as shown in Figure 7.

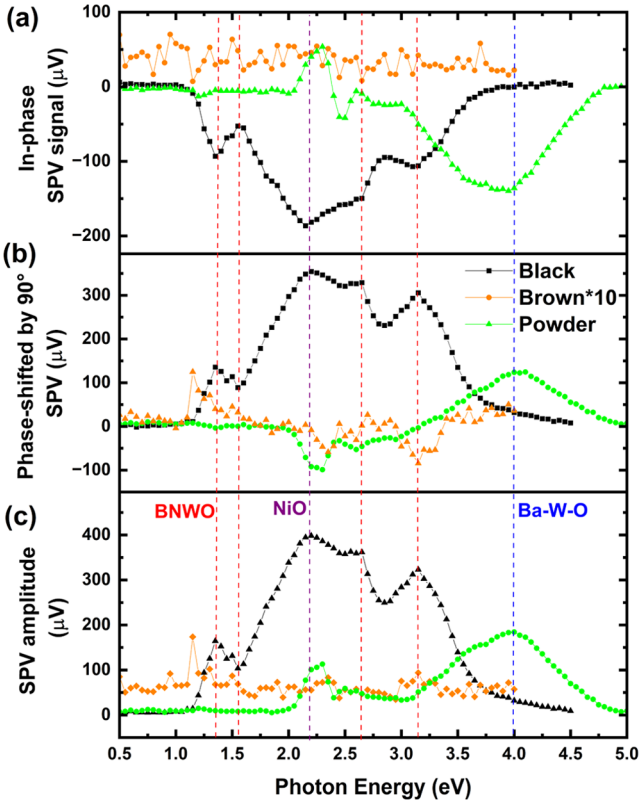

Figure 7. Surface photovoltage (SPV) measurement on the surface of BNWO black crystal (black), brown crystal (brown), and polycrystalline pellet (green) plotted as a function of photon energy; panel (a) represents the in-phase X component, panel (b) represents the phase-shifted by 90° (Y) component, and panel (c) represents the SPV amplitude (composed of both X and Y components). The dashed red lines represent the absorption of the BNWO phase in the black crystal and the corresponding shifts in the other samples. The blue and purple lines represent absorption peaks that might be attributed to the impurity phases Ba−W−O and NiO, respectively.

All three samples exhibit not only some similar spectral features but also notable variations in the intensity and fine structure. The brown crystal—with 0.26% NiO, 5.37% Ba_2WO_5, and 2.34% $BaWO_4$ impurities—has very weak absorption peaks in the range of 0.5−4 eV that appear only in the Y component, which was multiplicated by a factor of 20.

The most prominent features across all samples are sharp peaks at approximately 1.35, 2.25, 2.65, and 3.15 eV visible in both the X and Y components and consequently in the R signal (Figure 7a−c). This peak likely corresponds to a fundamental electronic transition within BNWO, possibly related to the band gap or a strong excitonic state. In the X component (Figure 7a), additional peaks are observed at around 1.60 eV and a dip in the 2.6−3.0 eV range. The intensity of these features decreases from the black sample to the powder sample and is least pronounced in the brown sample. In the powder sample, there is a change of sign for the excitation as well as a broad hump starting at 3.50 eV, suggesting different surface states, defect concentration, or possible impurities in the samples as summarized in Table 3.

Table 3. Comparison between the Optical Excitations of Double Perovskite Compounds Involved in This Work and the Reported Absorption for Impurity Phases

compound	optical absorption (eV)	impurities (%)
Ba_2NiWO_6 black	1.35, 60, 2.25, 2.65, 3.15	1.3% NiO
Ba_2NiWO_6 brown	1.25, 2.00, 2.60, 3.10	0.26% NiO, 5.37% Ba_2WO_5, 2.34% $BaWO_4$
Ba_2NiWO_6 powder	2.20, 3.30, 4.00	1.76 NiO, 5.98% $BaWO_4$
Ba_2CoWO_6 powder	2.32, 3.23[31]	
NiO	2.20, 3.60[30]	
Ba_2WO_5	3.17 (theoretical)[32]	
$BaWO_4$	3.08,[33] 4.88[34]	

The Y component (Figure 7b) reveals complex phase behavior, characterized by a sharp peak at 1.35 eV, followed by a broad region from approximately 1.5 to 2.5 eV, and a small positive peak at about 2.65 eV. Again, these features are most pronounced in the black sample and least evident in the brown sample. The magnitude of the SPV signal (Figure 7c) combines the X and Y components, showing clear peaks at 1.35, 2.25, 2.65, and 3.15 eV.

These results match with previous theoretical reports, suggesting indirect band gaps at 2.48 eV and semiconducting properties for BNWO.[7,29] Also, there is a wide band gap at 3.29 eV.[29] The peak at 2.20 eV could be attributed to NiO, which has optical absorption in this range.[30] Nevertheless, the isostructural double perovskite compound Ba_2CoWO_6 powder has also an absorption peak at 2.32 eV in the pure powder form.[31] Therefore, this peak is most probably attributed to the band structure of the BNWO.

The observed differences in SPV spectra among the three sample preparations of BNWO (black crystal, brown crystal, and powder) suggest that the growth atmosphere significantly influences the material's electronic structure and surface properties. The black sample consistently shows the most defined spectral features, indicating a higher degree of electronic order or stronger light−matter interactions. In contrast, the powder sample exhibits a more homogeneous response across the spectrum, possibly due to increased light scattering or a more averaged bulk response. In the brown crystal, the impurities are mainly Ba_2WO_5 and $BaWO_4$, which are insulators, and their absorption is between 3.08 and 4.88 eV (see Table 3).[32−34] These insulators might induce an internal electric field that slows the response of the sample to light absorption, which is indicated by the larger Y component.[18]

These results highlight the importance of sample preparation in determining the optoelectronic properties of BNWO. The variations in SPV spectra among the black, brown, and powder samples may be attributed to differences in surface states, defect concentrations, crystalline order, and impurities, all of which can significantly affect the material's

https://doi.org/10.1021/acs.cgd.4c01467
Cryst. Growth Des. 2025, 25, 1155−1163

light absorption and charge transport properties and its resulting photovoltage response. The impurities and structural defects can also produce multilevels in the fine structure, which alters the absorption spectrum.[35−37]

The photoactivity is quite well known for perovskite and double perovskite structures, with many interesting examples including Sr_2FeMoO_6[38] and $Ba_{0.5}Sr_{0.5}Co_{0.8}Fe_{0.2}O_{3-\delta}$.[39] Our work also provided clear evidence that the growth conditions affect the band gap, which might be tuned for different applications. Therefore, a more detailed investigation is needed to understand the mechanism of gap opening, defect engineering, and absorption tuning, which may provide considerable applications in photocatalysis and optoelectronic applications depending on the absorption spectrum and quantum efficiency.[5−7]

CONCLUSIONS

This study introduced the intriguing characteristics of double perovskite FCC lattice antiferromagnet Ba_2NiWO_6 (BNWO). Through comprehensive investigations encompassing crystal growth trials, structural analysis, physical property assessments, magnetic characterizations, and exploration of the electronic structure, we gained valuable insights into the magnetism exhibited by this class of double perovskites.

Our analysis revealed the effect of the growth atmosphere on the color of the sample, magnetic properties, and optical absorption. The magnetic characterization and heat capacity indicated that BNWO exhibited a conventional $J = S = 1$ ground state with a possible weak orbital contribution. The antiferromagnetic order onsets below $T_N = 47$ K, while the Curie−Weiss temperature is ∼100 K.

Surface photovoltage (SPV) spectroscopy revealed significant differences in the electronic properties and absorption spectra of three BNWO samples (black crystal, brown crystal, and powder). The brown crystal, which has various impurities, indicated very weak absorption peaks. In contrast, the black crystal exhibited multiple absorption peaks, suggesting semiconducting properties, while the powder sample had similar absorption characteristics with extra impurity peaks.

The results underscore that achieving high purity in BNWO crystals requires careful attention to growth conditions including temperature control, atmosphere, and impurity mitigation strategies. Our findings suggest that increasing the growth pressure with mixed argon and oxygen gases may stabilize the growth. Future research will focus on refining these techniques further to enhance crystal quality and explore additional methods for purification post growth. These findings contribute to a deeper understanding of how growth environments impact the structural integrity and functional properties of BNWO, paving the way for potential applications in quantum magnetism and optoelectronics.

ASSOCIATED CONTENT

Supporting Information

The Supporting Information is available free of charge at https://pubs.acs.org/doi/10.1021/acs.cgd.4c01467.

A ternary phase diagram of Ba_2NiWO_6 based on precursors (BaO, NiO, WO_3); images of failed growth trials under different conditions; X-ray powder diffraction (PXRD) data and Rietveld refinement results for powder and single-crystal samples; energy-dispersive X-ray (EDX) spectrometry analysis of atomic percentages in different samples; and X-ray photoelectron spectroscopy (XPS) spectra comparing brown and black crystals. This additional information provides further insights into the crystal growth process, structural analysis, and compositional characterization of Ba_2NiWO_6 samples. (PDF)

AUTHOR INFORMATION

Corresponding Authors

Abanoub R. N. Hanna − *Institut für Festkörperphysik, Technische Universität Berlin, 10587 Berlin, Germany; Helmholtz-Zentrum Berlin für Materialien und Energie, 14109 Berlin, Germany;* orcid.org/0000-0002-1077-6764; Email: Abanoub.Hanna@helmholtz-berlin.de

Bella Lake − *Institut für Festkörperphysik, Technische Universität Berlin, 10587 Berlin, Germany; Helmholtz-Zentrum Berlin für Materialien und Energie, 14109 Berlin, Germany*; Email: bella.lake@helmholtz-berlin.de

Authors

A. T. M. Nazmul Islam − *Helmholtz-Zentrum Berlin für Materialien und Energie, 14109 Berlin, Germany*

Daniel Abou-Ras − *Helmholtz-Zentrum Berlin für Materialien und Energie, 14109 Berlin, Germany;* orcid.org/0000-0003-3063-922X

Clemes Ritter − *Institut Laue-Langevin, 38042 Grenoble Cedex 9, France*

Igal Levine − *Institute of Chemistry and The Center for Nanoscience and Nanotechnology, The Hebrew University, Jerusalem 91904, Israel;* orcid.org/0000-0003-0406-2922

Ralf Feyerherm − *Helmholtz-Zentrum Berlin für Materialien und Energie, 14109 Berlin, Germany;* orcid.org/0000-0003-3034-4210

Complete contact information is available at: https://pubs.acs.org/10.1021/acs.cgd.4c01467

Notes

The authors declare no competing financial interest.

ACKNOWLEDGMENTS

The authors acknowledge the CoreLab Quantum Materials at Helmholtz Zentrum Berlin für Materialien und Energie (HZB), Germany, where the powder and single-crystal samples of Ba_2NiWO_6 were synthesized and measured. This work was also partly based on experiments performed at the Reactor Neutron Source Institut Laue-Langevin, Grenoble, France. The authors acknowledge Christian Höhn from the Institute of Solar Fuels, HZB, for performing the X-ray photoemission spectroscopy, and Thomas Dittrich from the Solar Energy Division, HZB, for performing the surface photovoltage measurements of BNWO. This research was supported by the Deutsche Forschungsgemeinschaft (DFG) through project B06 of the SFB 1143 (ID 247310070). The authors also acknowledge the CoreLab Quantum Materials (CLQM), Helmholtz Zentrum Berlin für Materialien und Energie (HZB), Germany, where the powder and single-crystal samples were synthesized, and the bulk thermodynamic and magnetic properties were measured.

REFERENCES

(1) Kobayashi, K. I.; Kimura, T.; Sawada, H.; et al. Room-temperature magnetoresistance in an oxide material with an ordered double-perovskite structure. *Nature* **1998**, *395* (6703), 677−680.

(2) Viola, M. C.; Martínez-Lope, M. J.; Alonso, J. A.; et al. Induction of Colossal Magnetoresistance in the Double Perovskite Sr2CoMoO6. *Chem. Mater.* **2002**, *14* (2), 812−818.

(3) Bijelić, J.; et al. Size reduction-induced properties modifications of antiferromagnetic dielectric nanocrystalline Ba2NiMO6 (M = W, Te) double perovskites. *Oxford Open Mater. Sci.* **2021**, *1* (1), No. itaa003, DOI: 10.1093/oxfmat/itaa003.

(4) Liu, S.; Cheng, Y.; Yan, S.; et al. Unravelling the Electromagnetic Behavior in Ordered Double-Perovskite Sr2FeMoO6. *J. Electron. Mater.* **2022**, *51* (7), 3430−3437.

(5) Vasala, S.; Karppinen, M. A2B′B″O6 perovskites: A review. *Prog. Solid State Chem.* **2015**, *43* (1), 1−36.

(6) Serrate, D.; Teresa, J. M. D.; Ibarra, M. R. Double perovskites with ferromagnetism above room temperature. *J. Phys.: Condens. Matter* **2007**, *19* (2), No. 023201.

(7) Rachedi, A.; Baghdad, R.; Nacef, A. Magnetic, optoelectronic and thermodynamic properties of the double perovskite Ba2NiWO6 in its stable antiferromagnetic phase. *Optik* **2021**, *227*, No. 166032.

(8) Yilmaz, H.; et al. Synthesis and optical properties of LaSrGaO4:RE3+ (RE = Sm, Eu, Ho) single crystals via optical float zone method. *Opt. Mater. X* **2025**, *25*, No. 100380, DOI: 10.1016/j.omx.2024.100380.

(9) Talapatra, A.; Uberuaga, B. P.; Stanek, C. R.; et al. A Machine Learning Approach for the Prediction of Formability and Thermodynamic Stability of Single and Double Perovskite Oxides. *Chem. Mater.* **2021**, *33* (3), 845−858.

(10) Guo, S.; Morrow, R.; van den Brink, J.; et al. Machine learning facilitated by microscopic features for discovery of novel magnetic double perovskites. *J. Mater. Chem. A* **2024**, *12* (10), 6103−6111.

(11) Yilmaz, H.; Küster, K.; Starke, U.; et al. Realization of a classical Ruddlesden Popper type bilayer nickelate in Sr3Ni2−xAlxO7−δ with unusual Ni4+. *npj Quantum Mater.* **2024**, *9* (1), No. 92, DOI: 10.1038/s41535-024-00708-5.

(12) Zhou, Y.; Yuan, D.; Víllora, E. G.; et al. High-density Nb:YTaO4 single crystals for X-ray scintillation. *CrystEngComm* **2024**, *27* (1), 81−89.

(13) Zhou, Y.; Yuan, D.; Nakauchi, D.; et al. Bulk crystal growth and characterization of intrinsic scintillator CaNb2O6. *J. Cryst. Growth* **2023**, *624*, No. 127432, DOI: 10.1016/j.jcrysgro.2023.127432.

(14) Nishikawa, A.; Ichiba, K.; Kato, T.; et al. Near-infrared scintillation properties of Nd-doped CaYAl3O7 single crystals. *Appl. Radiat. Isot.* **2024**, *214*, No. 111559, DOI: 10.1016/j.apradiso.2024.111559.

(15) Puphal, P.; Reiss, P.; Enderlein, N.; et al. Unconventional Crystal Structure of the High-Pressure Superconductor La3Ni2 O7. *Phys. Rev. Lett.* **2024**, *133* (14), No. 146002, DOI: 10.1103/PhysRevLett.133.146002.

(16) Martínez-Lope, M.; Alonso, J.; Casais, M. T. Synthesis, Crystal and Magnetic Structure of the Double Perovskites A2NiMoO6 (A = Sr, Ba): A Neutron Diffraction Study. *Eur. J. Inorg. Chem.* **2003**, *2003*, 2839−2844.

(17) Eriksson, A. K.; Eriksson, S. G.; Ivanov, S. A.; et al. Phase Transitions of the Magnetoelectric A2NiMoO6 (A = Ba, Sr) and Ca2NiWO6 by Neutron Diffraction. *Ferroelectrics* **2006**, *339* (1), 235−243.

(18) Levine, I.; Vera, O. G.; Kulbak, M.; et al. Deep Defect States in Wide-Band-Gap ABX3 Halide Perovskites. *ACS Energy Lett.* **2019**, *4* (5), 1150−1157.

(19) Khalyavin, D. D.; Han, J.; Senos, A.; et al. Synthesis and dielectric properties of tungsten-based complex perovskites. *J. Mater. Res.* **2003**, *18* (11), 2600−2607.

(20) Rodríguez-Carvajal, J. Recent advances in magnetic structure determination by neutron powder diffraction. *Physica B* **1993**, *192* (1), 55−69.

(21) Bhanuchandar, S.; Vinothkumar, G.; Arunkumar, P.; et al. Unravelling the role of cationic Ni2+ vacancies and Ni3+ ions in non-stoichiometric NiO: breakdown of anti-ferromagnetic ordering and large exchange bias. *J. Mater. Sci.* **2023**, *58*, 1−18, DOI: 10.1007/s10853-023-08853-1.

(22) Pointon, A. J.; Robertson, J.; Wetton, G. Anisotropy Of Ni2+ and Ni3+ Ions In Cubic Sites. *J. Phys. Colloques* **1971**, *32* (C1), C1-850−C1-852.

(23) Zheng, W.-C. Anisotropy of the g factor for Ni2+ and Ni3+ ions in the tetragonal phase of SrTiO3. *Phys. B* **1994**, *198* (4), 329−331.

(24) Srinivasan, G.; Seehra, M. S. Magnetic susceptibilities, their temperature variation, and exchange constants of NiO. *Phys. Rev. B* **1984**, *29* (11), 6295−6298.

(25) Todate, Y. Exchange interactions in antiferromagnetic complex perovskites. *J. Phys. Chem. Solids* **1999**, *60* (8), 1173−1175.

(26) Vasilchikova, T.; Vasiliev, A.; Evstigneeva, M.; et al. Magnetic Properties of A2Ni2TeO6 (A = K, Li): Zigzag Order in the Honeycomb Layers of Ni2+ Ions Induced by First and Third Nearest-Neighbor Spin Exchanges. *Materials* **2022**, *15* (7), 2563.

(27) Bogdanov, A. N.; Zhuravlev, A. V.; Rößler, U. K. Spin-flop transition in uniaxial antiferromagnets: Magnetic phases, reorientation effects, and multidomain states. *Phys. Rev. B* **2007**, *75* (9), No. 094425.

(28) Belhamra, S.; Masrour, R.; Hlil, E. K. Dynamic Phase Transitions, Electronic, and Magnetic Properties of Ba2NiWO6 and Sr2NiWO6 Double Perovskites. *J. Supercond. Novel Magn.* **2022**, *35* (12), 3613−3622.

(29) Alsabah, Y. A.; AlSalhi, M. S.; Elbadawi, A. A.; et al. Influence of Zn2+ and Ni2+ cations on the structural and optical properties of Ba2Zn1−xNixWO6 ($0 \leq x \leq 1$) tungsten double perovskites. *J. Alloys Compd.* **2017**, *701*, 797−805.

(30) Huck, N. R.; Smart, R. S. C.; Thurgate, S. M. Surface photovoltage and XPS studies of electronic structure in defective nickel oxide powders. *Surf. Sci. Lett.* **1986**, *169* (1), L245−L252.

(31) Hanna, A. R. N.; et al. Growth of Ba(2)CoWO(6)single crystals and their magnetic, thermodynamic and electronic properties. *J. Phys.: Condens. Matter* **2024**, *36* (50), No. 505801, DOI: 10.1088/1361-648X/ad7770.

(32) Ohad, G.; Gant, S. E.; Wing, D.; et al. Optical absorption spectra of metal oxides from time-dependent density functional theory and many-body perturbation theory based on optimally-tuned hybrid functionals. *Phys. Rev. Mater.* **2023**, *7* (12), No. 123803.

(33) Talebi, R. Synthesis and characterization of BaWO4 nanoparticles with the aid of different surfactants and their photocatalyst properties. *J. Mater. Sci.: Mater. Electron.* **2017**, *28* (9), 6782−6787.

(34) Stephen, S. K.; Ganesh, S.; Varghese, T. Modifications of structural and optical properties of nanophase BaWO4 phosphors: Dose dependent effect of high energy electron beam irradiation. *Radiat. Phys. Chem.* **2021**, *180*, No. 109317.

(35) Qiao, L.; Bi, X. Direct observation of Ni3+ and Ni2+ in correlated LaNiO3−δ films. *Europhys. Lett.* **2011**, *93* (5), No. 57002.

(36) Vasileva, N. V.; Gerus, P. A.; Sokolov, V. O.; et al. Optical absorption of Ni2+ and Ni3+ ions in gadolinium gallium garnet epitaxial films. *J. Phys. D: Appl. Phys.* **2012**, *45* (48), No. 485301.

(37) D'Amario, L.; Föhlinger, J.; Boschloo, G.; et al. Unveiling hole trapping and surface dynamics of NiO nanoparticles. *Chem. Sci.* **2018**, *9* (1), 223−230.

(38) Li, X. Y.; Yao, Z. F.; Zhang, L. Y.; et al. Generation of oxygen vacancies on Sr2FeMoO6 to improve its photocatalytic performance through a novel preparation method involving pH adjustment and use of surfactant. *Appl. Surf. Sci.* **2019**, *480*, 262−275.

(39) Tang, L.; Zhang, W.; Lin, D.; et al. The hexagonal perovskite Ba0.5Sr0.5Co0.8Fe0.2O3−δ as an efficient electrocatalyst for the oxygen evolution reaction. *Inorg. Chem. Front.* **2020**, *7* (22), 4488−4497.

https://doi.org/10.1021/acs.cgd.4c01467
Cryst. Growth Des. 2025, 25, 1155−1163